Nuclear Engineering and Technology 54 (2022) 997–1002

Contents lists available at ScienceDirect

Nuclear Engineering and Technology

journal homepage: www.elsevier.com/locate/net

Original article

Partitioning effects and corrosion characteristics of oxyapatite glass-ceramic wasteforms sequestering rare-earth elements

Miae Kim [a, b], Jaehyuk Kang [a], Jang-Hee Yoon [b], Sang-Geul Lee [c], Wooyong Um [a, **], Hyun Gyu Kim [b, *]

[a] Division of Advanced Nuclear Engineering, Pohang University of Science and Technology, Pohang, 37673, South Korea
[b] Busan Centre, Korea Basic Science Institute, Busan 46742, South Korea
[c] Daegu Centre, Korea Basic Science Institute, Daegu 41566, South Korea

ARTICLE INFO

Article history:
Received 11 April 2021
Received in revised form
2 August 2021
Accepted 30 August 2021
Available online 4 September 2021

Keywords:
Corrosion
Apatite
Glass ceramics
Nuclear applications

ABSTRACT

Oxyapatite[$Ca_2Nd_8(SiO_4)_6O_2$] glass-ceramics have been suggested as wasteforms for the immobilisation of rare-earth radioactive nuclides because of their high waste-loading capability and good chemical durability. In particular, a partitioning effect is predicted to contribute to an enhancement of corrosion resistance in glass-ceramics compared with that of conjugate glasses of the same composition. Because rare-earths are inherently insoluble nuclides, detection of changes in corrosion behavior between glass-ceramics and conjugate glasses under normal conditions is not easy. In this study, therefore, we revealed the partitioning effect by exposing glass-ceramics and glasses to solution of pH 2, 7 and 10 at 90 °C for 20 d. In addition, we proposed the corrosion mechanism for oxyapatite glass-ceramics under various corrosion conditions. Especially, the glassy phase dissolved first, followed by the oxyapatite phase during pH 7 corrosion.

1. Introduction

Rare-earth (RE) radioactive wastes have been generated by reprocessing [1] and pyro-chemical processing [2] of spent fuels, and various materials such as glasses [3,4], glass-ceramics (GCs) [5], and ceramics [6] have been studied for the purpose of RE immobilisation. GCs have an amorphous phase and one or more crystalline phases and are produced by controlled crystallisation. GCs have been considered as wasteforms for RE because they have the fabrication advantage of glass, as well as the special properties of ceramics, such as high RE loading and good corrosion durability [7–9]. In particular, oxyapatite GCs are known to exhibit high RE loadings and chemical durability [10–12].

The corrosion advantage of GCs as a wasteform compared with that of glasses or ceramics occurs by way of partitioning effect [13]. Here, partitioning refers to the structure in which RE nuclides are incorporated in crystals and glasses, and encapsulated by glass. That is, according to McCloy and Goel [13], chemical incorporation occurs at the atomic scale, whereas encapsulation involves embedding or physical sequestration at the macro-scale. The partitioning of GCs would have the effect of improving corrosion durability, because the amorphous phase could serve as an additional barrier in the event that elements including RE nuclides leach out of the crystal. In addition to partitioning effect, the oxyapatite phase has high RE loading and high chemical durability compared to the glass matrix [14,15]. That's why we selected oxyapatite[$Ca_2Nd_8(SiO_4)_6O_2$] crystal-containing GCs as wasteforms for sequestering RE. In this study, we attempted to identify the partitioning of oxyapatite GCs directly through elemental mapping, and revealed the corrosion behaviors of the GC in various pH environment.

Oxyapatite GCs exhibit hexagonal-structured crystals, which appear as dendrites [9]. If oxyapatite GCs are well-partitioned, theoretically, the leaching of the target elements such as Ce and Nd from the GCs to aqueous environments should be retarded compared to those from the glasses. However, we could not compare the released values between glass and GC from the published leaching data (pH 7, 90 °C, 20 d) because the released concentrations of Nd and Ce were less than the analysis limit of inductively coupled plasma mass spectrometry [7]. Thus, we attempted to intentionally increase the leaching amount of the

* Corresponding author.
** Corresponding author.
E-mail addresses: wooyongum@postech.ac.kr (W. Um), hhgkim@kbsi.re.kr, kmapl@postech.ac.kr (H.G. Kim).

https://doi.org/10.1016/j.net.2021.08.036

glass and GCs through exposure to a harsh solution environment. Then, we investigated the effect of improving the corrosion durability of the GCs compared with that of the glasses. In addition, we attempted to investigate the corrosion behaviours of the hexagonal structural oxyapatite GCs.

2. Materials and methods

The specimens were prepared according to the methods or conditions described in the previous study by Kim et al. [9]. The glasses with a composition of 46SiO_2 - 12Na_2O - 12B_2O_3 - 24CaO - 3CeO_2 - 3Nd_2O_3 (mol%) was made by melting at 1300 °C for 30 min. It was devitrified by heat treatment at 750 °C for 3 h. The glasses and GCs were cut to monoliths with a size of 10 × 10 × 2 mm and polished on both 10 × 10 mm faces. To expose these specimens to harsh dissolution conditions, a leaching solution was prepared under a fume hood by mixing 1 M HCl with deionised(DI)-water, for a pH 2 solution and 1 M NaOH with DI-water for a pH 10 solution. Pure DI-water was used as the pH 7 solution because measured pH of the DI-water was 6.7 under fume hood. The exposed time of the DI-water to air was adjusted within 1 min to prevent lowering pH of the water by minimizing CO_2 absorption. Each specimen was placed on a net-shaped Teflon holder in a Teflon vessel with solutions of pH 2, 7, and 10. Each vessel contained a glass surface to solution volume ratio of 10 m^{-1} and was stored at 90 °C for 20 d.

The solution after corrosion was sampled with a 45 μm filter to measure the pH and analyse the leached elemental concentrations through inductively coupled plasma optical emission spectrometry (ICP-OES, Activa, Horiba JY). The specimens after corrosion were subjected to X-ray diffraction (XRD, PANalytical, EMPYREAN) measurements with 40 V of generator voltage and 25 mA of tube current without further polishing. From the XRD pattern, relative weight fractions of phases of all specimens were analysed using Highscore software applying direct derivation algorithm [16]. In addition, they underwent Pt coating (40 mA for 30 s) followed by secondary electron microscopy with 10 kV (SEM, JEOL, JSM-7401F). To identify the partitioning effect, the polished GC before the corrosion experiment was Pt-coated, and energy dispersive spectroscopy (EDS, JEOL, JSM-7401F) was performed. The specimens after the corrosion test were named after the specimen type (Glass (G) or Glass-ceramics (GC)) along with the pH condition of the corrosion test. For example, GC2 refers to GC specimens exposed to the pH 2 acidic solution.

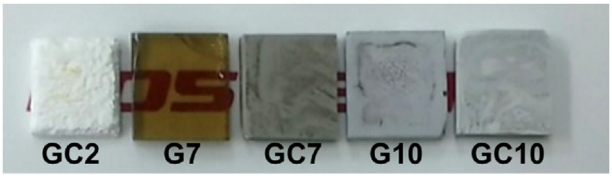

Fig. 2. Appearance of the specimens after the corrosion experiments under various pH conditions for 20 d at 90 °C. Note that a picture for the G2 could not be taken, because it was fragmented during the corrosion experiment.

3. Results and discussion

3.1. Partitioning effect of the oxyapatite glass-ceramics

Fig. 1 shows the EDS elemental mapping of the GCs before dissolution. The upper-left part in Fig. 1 shows the SEM image of a calcium neodymium (cerium) oxide silicate [$Ca_2Nd_{8-x}Ce_x(SiO_4)_6O_2$] crystal and the others, showing the concentration mappings of many elements, such as Si, Na, O, Ca, Nd, and Ce over the crystal. The colours of Si, Na, and O in the crystalline phase are darker than those in the glass matrix, which means that these elements are depleted in the crystal. Even though Si and O are contained in the crystalline phase based on the crystalline formula, they are still or even more contained in the matrix phase when calculated from the glass composition. For Na, the interpretation of the result should be done carefully because unintended migration could be occurred under an electron beam during EDS measurement [14]. These elements might play a substantial role in the amorphous phase: Si as a glass network former and Na as a network modifier. Here, network formers mean main constituents of glasses and they form a highly cross-linked network of chemical bonds. And modifiers mean additives for modifying the glass properties by breaking the strongly bonded network in glasses [17]. Meanwhile, Nd and Ce are concentrated inside the crystal, which coincides with the preliminary results: 45 wt% of RE was concentrated inside the crystalline phases, which is 2.6-fold higher than the value in the glassy phase [9]; however, this represents only the numerical data. The

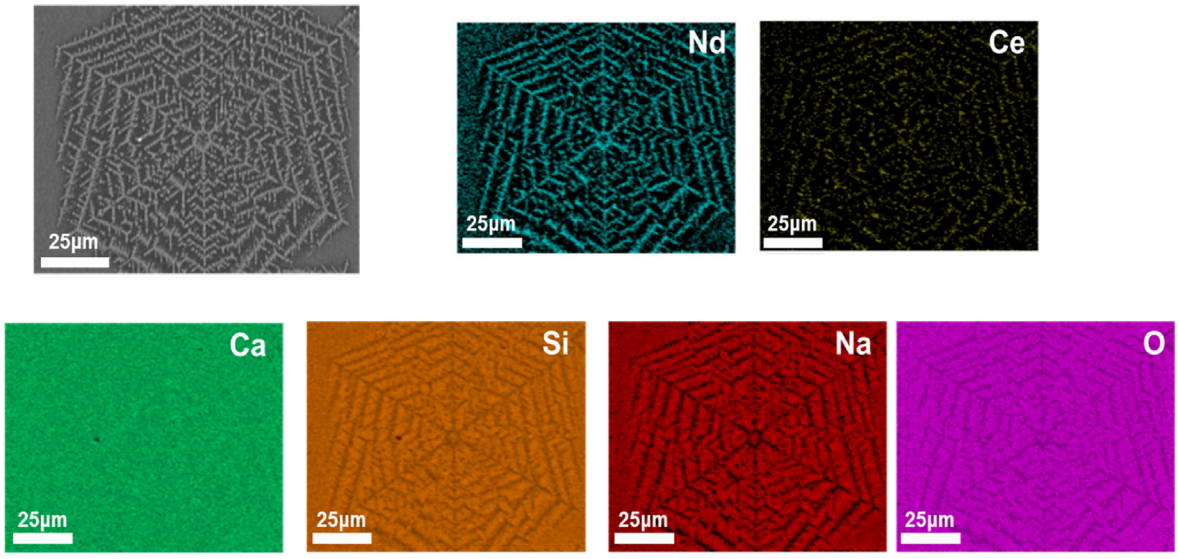

Fig. 1. Nd, Ce, Ca, Si, Na, and O elemental mapping of an oxyapatite crystal and neighbouring glassy phase on the oxyapatite GCs, fabricated by heat treatment of the conjugate G at 750 °C for 3 h, which was measured by energy dispersive spectrometry.

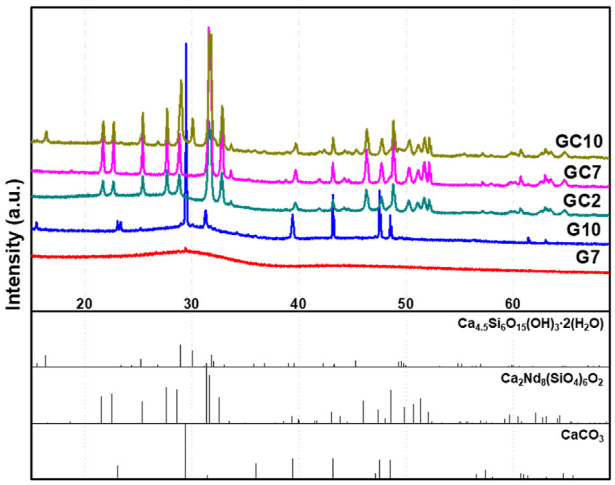

Fig. 3. X-ray diffraction patterns obtained from the surface of the specimens after immersion in various pH solutions for 20 d at 90 °C. Note that the G2 could not be measured, because it was fragmented during the corrosion experiment.

Table 1
The relative weight fraction (%) of phases of all specimens after corrosion test obtained by direct derivation algorithm [16].

	Amorphous	Oxyapatite	Tobermorite	Calcite	Total
GC2	44.0	56.0	–	–	100.0
GC7	24.9	75.1	–	–	100.0
GC10	21.4	47.2	31.4	–	100.0
	[a](31.2)	[a](68.8)	[a](0.0)		[a](100.0)
G2	100.0	–	–	–	100.0
G7	100.0	–	–	–	100.0
G10	44.5	–	35.4	20.1	100.0

[a] ( ): Relative fraction of phases assuming that only oxyapatite and amorphous phases exist in GC10.

EDS mapping results in this study are the direct and intuitive evidence of the partitioning of the target elements of the oxyapatite GC. Concentrations of Ca cannot be distinguished between the two sides, which means that similar concentration of Ca are represented in both phases.

3.2. Appearance of the specimens after the corrosion

Fig. 2 shows the appearance of the specimens after immersion in the pH 2, 7, and 10 solutions for 20 d. Original glasses showed a transparent light brown colour, probably because of the presence of Ce^{4+} and Nd^{3+} ions, and after the 3 h heat treatment at 750 °C, the specimens became opaque with a grey colour [9]. The specimens immersed in pH 7 solution (G7 and GC7) showed almost no colour change, which may signify minor surface changes due to contact with the pH 7 solution. Except for G7, all the other glasses were altered by the harsh conditions of this experiment. G10 and GC10 turned lighter grey overall, and arbitrary patterns consisting of white spots and grey parts were evident. The most remarkable change was shown in G2 and GC2. Both were altered to be more brittle and completely changed their original colours into white. A picture of G2 could not be taken because it was fragmented during the corrosion test in the acidic solution. This shows that these specimens are chemically weaker in the acidic environment than in the basic environment.

3.3. Surface precipitation after the corrosion

Fig. 3 shows the XRD patterns obtained from the surface of the G and GCs after the corrosion test. In G2 and G7, no crystals formed. Patterns obtained from the GC2, GC7, and GC10 after the corrosion test matched with those of the Ca-Nd-silicate crystal [$Ca_2Nd_8(SiO_4)_6O_2$, oxyapatite, PDF #: 78-1038, hexagonal, $P6_3/m$], which shows the same crystals that formed in the GC before the corrosion test. This means that oxyapatite is still maintained, even under the conditions of harsh acidic or basic leachate without a phase disappearance. On the other hand, additional peaks were detected from XRD pattern of G10 and GC10. For GC10, calcium silicate hydrate mineral [$Ca_{2.25}Si_3O_{7.5}(OH)_{1.5}(H_2O)$, tobermorite, PDF #: 83-1520, orthorhombic, *Imm*2] were additionally formed in addition to the oxyapatite phases. The tobermorite were known to one of the secondary phases formed during alteration of representative waste glasses such as international simple glass(ISG) and SON68 [18,19]. In addition to the tobermorite phase, calcite crystals [$CaCO_3$, PDF#: 86-0174, hexagonal, R-3c] formed as a major phases on the G10 surface. These crystals are known to precipitate easily in alkaline environments [20].

Table 2
Normalized elemental mass release NL_i [$g{\cdot}m^{-2}$] and dissolution rate r_i [$g{\cdot}m^{-2}{\cdot}d^{-1}$] calculated from the concentration C_i [ppm] of element i in solution from the dissolution experiment for 20 days at 90 °C. Elements in the leachate were measured by ICP-OES. Error: ± 0.1%.

Specimens		Elements					
		Ce	Nd	Si	B	Na	Ca
G2	C_i	1413.70	2538.86	138.89	814.35	1770.09	3504.44
	NL_i	1463.29	1276.43	46.76	1365.74	1395.85	1585.16
	r_i	73.16	63.82	2.33	68.28	69.79	79.25
GC2	C_i	1324.61	2510.21	139.75	793.52	1732.64	3432.20
	NL_i	1371.07	1262.02	47.05	1330.81	1366.32	1552.49
	r_i	68.55	63.10	2.35	66.54	68.31	77.62
G7	C_i	[a]LoD	[a]LoD	14.94	4.42	10.68	10.07
	NL_i	–	–	5.03	7.41	8.42	4.55
	r_i	–	–	0.25	0.37	0.42	0.22
GC7	C_i	[a]LoD	[a]LoD	18.21	4.20	11.06	10.04
	NL_i	–	–	6.13	7.04	8.72	4.54
	r_i	–	–	0.30	0.35	0.43	0.22
G10	C_i	[a]LoD	[a]LoD	87.75	42.82	22344.19	[a]LoD
	NL_i	–	–	29.54	71.81	17620.14	–
	r_i	–	–	1.47	3.59	881.01	–
GC10	C_i	[a]LoD	[a]LoD	84.38	37.25	21983.04	[a]LoD
	NL_i	–	–	28.41	62.47	17335.35	–
	r_i	–	–	1.42	3.12	866.76	–

[a] LoD: limit of detection (<0.1 ppm) of ICP-OES.

The relative weight fractions of phases of all specimens after the corrosion test were listed in Table 1. Basically, glass specimens including G2 and G7 consist of only amorphous phase even after corrosion. However, 25.4% tobermorite and 20.1% calcite additionally formed in G10 due to the alkaline solution regardless of existence of the oxyapatite phase in the specimen. For GC specimens, oxyapatite of 56.0% in GC2 and of 75.1% in GC7 was present as only crystalline phase. 31.4% tobermorite were additionally formed during corrosion test in addition to 47.2% oxyapatite and 21.4% amorphous phase. But for GC10, even though 31.4% tobermorite were additionally formed during corrosion test, we recalculated the phase fractions of GC10 assuming that only oxyapatite crystals exist in GC10 for clear comparison with other GC specimens. As a result, the remaining fraction of oxyapatite phase among GCs was in the order of GC7(75.1%) > GC10 (68.8%) > GC2(56.0%) and fraction of amorphous phase showed the reverse order of that of oxyapatite.

3.4. Corrosion characteristics from released elemental concentration

Table 2 represents the normalized elemental mass release NL_i [$g \cdot m^{-2}$] and dissolution rate r_i [$g \cdot m^{-2} \cdot d^{-1}$] calculated from the concentration C_i [ppm] of element i in solution from the dissolution experiment for 20 days at 90 °C. The released concentrations of Ce and Nd measured after the corrosion test in pH 7 and 10 were still less than the detection limit of ICP-OES. However, in pH 2 solution, the released Ce and Nd amounts were higher than the detection limits. There was certainly significant elemental release at pH 2, and both glass and GC were more vulnerable to acidic leachate than to the other two solutions.

As the released amounts of the target elements were above the limits at pH 2, we could compare the corrosion properties between the G and the GC, at least for acidic case, as intended. The normalized releases of Ce were 1463 g m^{-2} for the G and 1371 g m^{-2} for the GC, and those of Nd were 1276 g m^{-2} for the G and 1262 g m^{-2} for the GC. Although it was not a big difference, the corrosion of Ce and Nd in the GCs were shown to decrease compared with the non-partitioned G (Error: ± 0.1%), which is consistent with our prediction.

Other elements such as Si, B, and Na in both the glass and the GC exhibited U-shaped behaviour, which was considered as general pH-dependent behaviours in glass [21,22]. The released amounts of Si and B were in the order of pH 2 > pH 10 > pH 7; however, the difference between the glass and the GC at each pH of these elements was not large. The major components of the glassy matrix, Si and B, are more vulnerable to the acidic environment than to the basic environment. Meanwhile, Na was in the order of pH 10 > pH 2 > pH 7. The reason for the high Na concentration in pH 10 is that NaOH was already included in the basic solution. Thus, the released behaviour of the Na leached from the G10 and GC10 specimens itself would be similar to that of Si and B. Uniquely, the Ca concentration was revealed to be below the detection limits in the pH 10 environment. That could be why the Ca, leached from the specimen to the solution, was re-consumed by re-precipitation on the specimen surface as a secondary phase, not remaining in the solution along with the other elements. That is compatible with the formation of calcite [$CaCO_3$] on G10 from the XRD results.

3.5. Surface alteration after the corrosion

Fig. 4 represents the SEM micrographs measured from the glasses and GCs after the corrosion test. The G7 surface was homogeneous, even after the corrosion experiments, which seemed to be almost same as that of the un-leached glass. The surface of GC7 was ordinary flat (as shown in the previous paper [7]) because it was polished prior to the corrosion. After the corrosion, notably, the difference in height between the glassy matrix and the oxyapatite phase was clearly apparent. Oxyapatite crystalline phases on the GC seem to be more resistant against corrosion than the glassy phase in the GC.

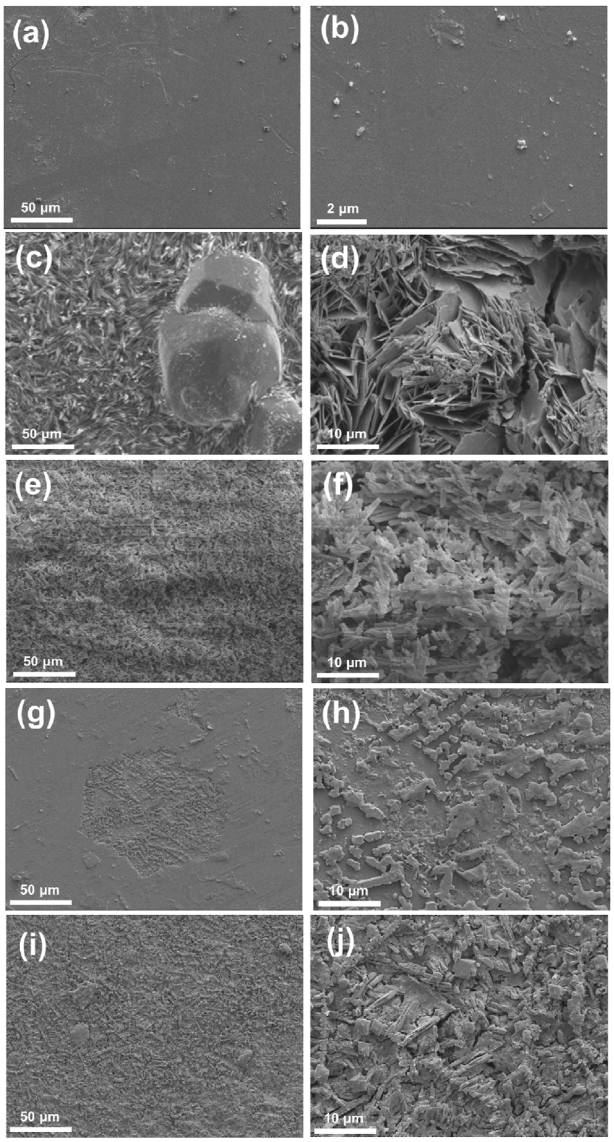

Fig. 4. Scanning electron micrographs of surfaces of (a-b) G7, (c-d) G10, (e-f) GC2, (g-h) GC7, and (i-j) GC10 after corrosion for 20 d at 90 °C. Note that the G2 could not be measured, because it was fragmented during the corrosion experiment.

On the surface of G10, something appeared to precipitates with a rock shape and platy shape (Fig. 4c and d). The rock shaped crystals with around 80 - 90 μm was found to be calcite, based on the XRD and EDS results (see supporting materials). The other crystals seem to be tobermorite, the image of which is well matched with previously published results [23]. The surface structures of GC2 and GC10, measured from XRD, were oxyapatite phases, but they were fragmented to a few μm, unlike what was formed with the so-called dendrite -shape of size greater than 100 μm before the corrosion. The extreme pH solution is also more unstable compared with the neutral condition, not only for glass but also for GC. Broken residues of GC2 seems to be fainter than those of GC10.

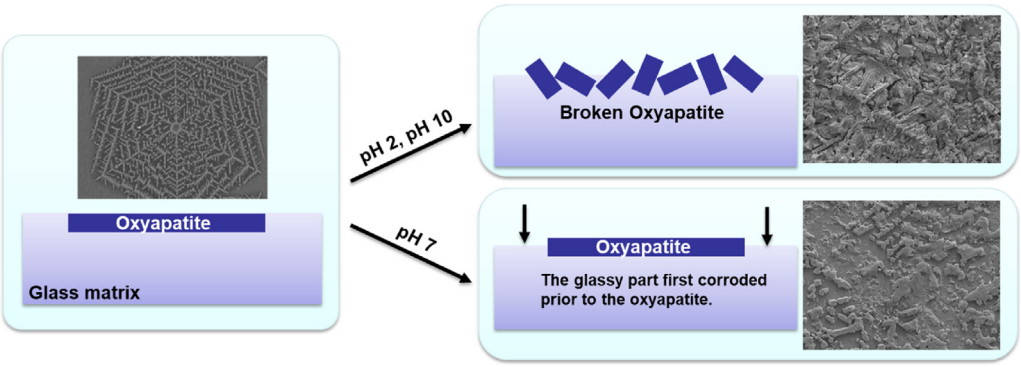

Fig. 5. Schematic diagram of corrosion behaviours in oxyapatite glass-ceramics immersed in various pH solutions at 90 °C for 20 d.

3.6. Corrosion mechanisms of the oxyapatite glass-ceramics

Based on the results we obtained, we suggest the corrosion mechanism of the oxyapatite GCs for the various pH conditions (Fig. 5). When the oxyapatite GCs were immersed in the pH 2 or pH 10 solutions at 90 °C for 20 d, oxyapatite crystals were broken to pieces, losing their dendrite shape during the corrosion experiments, based on the SEM data; however, their hexagonal crystal structures were maintained without changes, based on the XRD patterns. Meanwhile, in the moderate case such as DI-water, the overall dendrite-shape of the oxyapatites still remained, even though some portions of the crystalline phases were broken. Corrosion of the oxyapatites and glassy phase in the GC did not occur at the same rate; however, based on the height difference between the two phases, we found that the glassy phase dissolved first and the oxyapatite later. In terms of the elemental concentrations of the pH 7 leachate, the released concentration in both the glass and the GC are similar. Therefore, the total released amounts of the glass and the GC are similar; however, the glass is leached as a whole, and the GC appears to leach first from the glassy phase prior to the oxyapatite. As we extend the corrosion time further, we need to investigate how this mechanism would progress.

If we roughly calculate and compare the RE weight fraction in the G7 and the GC7, we can obtain the RE element fraction of G7 (~29%) from previous study [7], the RE element fraction inside oxyapatite phase of GC7 (~34% (= 75% (the fraction of oxyapatite phase from XRD in Table 1) * 45% (the RE weight fraction of oxyapatite phase from EDS of previous study [7])) and that inside amorphous phase of GC7 (~5% (= 25% (the fraction of amorphous phase from XRD in Table 1) * 18% (the RE weight fraction of amorphous phase from EDS of previous study [7])). Based on this calculation, assuming the released RE concentrations of the G7 and the GC7 are the same, it can be calculated that the ratio of the leached thickness (the thickness difference between specimen before and after corrosion) of the G7, the oxyapatite crystalline phase of GC7 and the amorphous phase of GC7 is 5:24:10 to satisfy equation 34%*5 + 5%*24 = 29%*10.

Although the advantages of GC-wasteforms have been suggested in terms of the simple manufacturing process and good chemical durability in theory, in practice, it is not well proven whether or not the corrosion durability of GC is improved compared to glass [24]. However, this study reveals why the corrosion characteristics of the target elements such as REs in the GC, which is easily manufactured only by additional heat treatment, are improved over those of glasses. That is, because the corrosion resistance of the crystalline phase containing the target elements in the GC is better than that of the glass matrix, it has been visually proven that the outflow of the nuclides incorporated in the crystalline phase can be delayed. Especially, this visual microscopic analysis of our study distinguish this study from previous references [22].

4. Conclusions

First, we visually demonstrated the partitioning of rare-earth elements in oxyapatite GCs. Ce and Nd had greater concentrations in the oxyapatite phase than in the amorphous matrix phase, whereas the other elements were depleted in the oxyapatite phase. To investigate the effect of partitioning on the corrosion of the GCs, we exposed the specimens to acid (pH 2) and basic (pH 10) solutions and performed a corrosion test. Results showed that the released values of Ce and Nd from the GCs were lower than those from the glasses when immersed in the pH 2 solution. In addition, G7 remained as a transparent and homogeneous glass, even after the corrosion test. However, calcite and tobermorite phases were precipitated on G10. For all the GC specimens, oxyapatite crystals survived during the corrosion test. However, the dendrite shapes of the oxyapatite were broken in the GC2 and GC10 samples, even though the shapes on GC7 survived. During the corrosion of the oxyapatite GCs in pH 7, the glassy phase dissolved first, followed by the oxyapatite phase.

Declaration of competing interest

The authors declare that they have no known competing financial interests or personal relationships that could have appeared to influence the work reported in this paper.

Acknowledgement

This research was supported by 'NST*-KBSI† Postdoctoral Research Fellowship for Young Scientists' at KBSI† in South KOREA. (*National Research Council of Science & Technology/†Korea Basic Science Institute) A portion of research was supported by the National Research Foundation of Korea (NRF), (NRF-2017M2B2B1072374 and NRF-2017M2B2B1072404). This work was supported by Busan Metropolitan City, Korea, Grant No. PO2019057and Korea Basic Science Institute Grant C140320.

References

[1] I. Bardez, D. Caurant, F. Ribot, P. Loiseau, J. Dussossoy, F. Villain, N. Baffier, C. Fillet, Structural characterisations of rare earth-rich glasses for nuclear waste immobilisation, Mater. Res. Soc. Symp. Proc. 807 (2003), https://doi.org/10.1557/PROC-807-157.
[2] J. Colombani, The alkaline dissolution rate of calcite, J. Phys. Chem. Lett 7 (2016) 2376–2380, https://doi.org/10.1021/acs.jpclett.6b01055.
[3] J. Crum, V. Maio, J. McCloy, C. Scott, B. Riley, B. Benefiel, J. Vienna, K. Archibald,

C. Rodriguez, V. Rutledge, Z. Zhu, J. Ryan, M. Olszta, Cold crucible induction melter studies for making glass ceramic waste forms: a feasibility assessment, J. Nucl. Mater. 444 (2014) 481–492, https://doi.org/10.1016/j.jnucmat.2013.10.029.

[4] J.V. Crum, L. Turo, B. Riley, M. Tang, A. Kossoy, Multi-phase glass-ceramics as a waste form for combined fission products: alkalis, alkaline earths, lanthanides, and transition metals, J. Am. Ceram. Soc. 95 (2012) 1297–1303, https://doi.org/10.1111/j.1551-2916.2012.05089.x.

[5] A. Jarošíková, V. Ettler, M. Mihaljevič, B. Kříbek, B. Mapani, The pH-dependent leaching behavior of slags from various stages of a copper smelting process: environmental implications, J. Environ. Manage. 187 (2017) 178–186, https://doi.org/10.1016/j.jenvman.2016.11.037.

[6] M. Kim, J. Heo, Vitusite glass-ceramics wasteforms for immobilization of lanthanide wastes generated by pyro-processing, Ceram. Int. 41 (2015) 6132–6136, https://doi.org/10.1016/j.ceramint.2015.01.035.

[7] M. Kim, J. Heo, Calcium-borosilicate glass-ceramics wasteforms to immobilize rare-earth oxide wastes from pyro-processing, J. Nucl. Mater. 467 (2015) 224–228, https://doi.org/10.1016/j.jnucmat.2015.09.040.

[8] M. Kim, C.L. Corkhill, N.C. Hyatt, J. Heo, Development, characterization and dissolution behavior of calcium-aluminoborate glass wasteforms to immobilize rare-earth oxides, Sci. Rep. 8 (2018) 5320, https://doi.org/10.1038/s41598-018-23665-z.

[9] M.A. Kim, J.H. Song, W. Um, N. Hyatt, S.-K. Sun, J. Heo, Structure analysis of vitusite glass–ceramic waste forms using extended x-ray absorption fine structures, Ceram. Int. 43 (2017) 4687–4691, https://doi.org/10.1016/j.ceramint.2016.12.129.

[10] N.A. Krishnan, S. Mangalathu, M.M. Smedskjaer, A. Tandia, H. Burton, M. Bauchy, Predicting the dissolution kinetics of silicate glasses using machine learning, J. Non-Cryst. Solids 487 (2018) 37–45, https://doi.org/10.1016/j.jnoncrysol.2018.02.023.

[11] I. Kumari, B. Kumar, A. Khanna, A review on UREX processes for nuclear spent fuel reprocessing, Nucl. Eng. Des. 358 (2020), 110410, https://doi.org/10.1016/j.nucengdes.2019.110410.

[12] W. Lee, M. Ojovan, M. Stennett, N. Hyatt, Immobilisation of radioactive waste in glasses, glass composite materials and ceramics, Adv. Appl. Ceram. 105 (2006) 3–12, https://doi.org/10.1179/174367606X81669.

[13] J.S. McCloy, A. Goel, Glass-ceramics for nuclear-waste immobilization, MRS Bull. 42 (2017) 233–240, https://doi.org/10.1557/mrs.2017.8.

[14] S. Gin, P. Jollivet, M. Tribet, S. Peuget, S. Schuller, Radionuclides containment in nuclear glasses: an overview, Radiochim. Acta 105 (2017) 927–959, https://doi.org/10.1515/ract-2016-2658.

[15] B. Karmakar, K. Rademann, A.L. Stepanov, Glass Nanocomposites: Synthesis, Properties, and Applications, William Andrew, 2016.

[16] H. Toraya, A new method for quantitative phase analysis using X-ray powder diffraction data: direct derivation of weight fractions from observed integrated intensities and chemical compositions of the individual phases, J. Appl. Crystallogr. 49 (2016) 1508–1516, https://doi.org/10.1107/S1600576716010451.

[17] M.M. Smedskjaer, J.C. Mauro, R.E. Youngman, C.L. Hogue, M. Potuzak, Y. Yue, Topological principles of borosilicate glass chemistry, J. Phys. Chem. B 115 (2011) 12930–12946, https://doi.org/10.1021/jp208796b.

[18] J. Neeway, A. Abdelouas, B. Grambow, S. Schumacher, C. Martin, M. Kogawa, S. Utsunomiya, S. Gin, P. Frugier, Vapor hydration of SON68 glass from 90°C to 200°C: a kinetic study and corrosion products investigation, J.non-cryst. Solid. 358 (2012) 2894–2905, https://doi.org/10.1016/j.jnoncrysol.2012.07.020.

[19] A. Abdelouas, Y.E. Mendili, A.A. Chaou, G. Karakurt, C. Hartnack, J.-F. Bardeau, T. Saito, H. Matsuzaki, A preliminary investigation of the ISG glass vapour hydration, Int. J. Appl. Glass Sci. 4 (2013) 307–316, https://doi.org/10.1111/ijag.12055|.

[20] S. Mohd Fadzil, P. Hrma, M.J. Schweiger, B.J. Riley, Liquidus temperature and chemical durability of selected glasses to immobilize rare earth oxides waste, J. Nucl. Mater. 465 (2015) 657–663, https://doi.org/10.1016/j.jnucmat.2015.06.050.

[21] J.A. Peterson, J.V. Crum, B.J. Riley, R.M. Asmussen, J.J. Neeway, Synthesis and characterization of oxyapatite [$Ca_2Nd_8(SiO_4)_6O_2$] and mixed-alkaline-earth powellite [(Ca,Sr,Ba)MoO_4] for a glass-ceramic waste form, J. Nucl. Mater. 510 (2018) 623–634, https://doi.org/10.1016/j.jnucmat.2018.08.048.

[22] J.J. Neeway, R.M. Asmussen, E.M. McElroy, J.A. Peterson, B.J. Riley, J.V. Crum, Kinetics of oxyapatite [$Ca_2Nd_8(SiO_4)_6O_2$] and powellite [(Ca,Sr,Ba)MoO_4] dissolution in glass-ceramic nuclear waste forms in acidic, neutral, and alkaline conditions, J. Nucl. Mater. 515 (2019) 227–237, https://doi.org/10.1016/j.jnucmat.2018.12.043.

[23] N.Y. Mostafa, A.A. Shaltout, H. Omar, S.A. Abo-El-Enein, Hydrothermal synthesis and characterization of aluminium and sulfate substituted 1.1 nm tobermorites, J. Alloys Compd. 467 (2009) 332–337, https://doi.org/10.1016/j.jallcom.2007.11.130.

[24] Z. Tian, J. Zhang, L. Zheng, W. Hu, X. Ren, Y. Lei, J. Wang, General trend on the phase stability and corrosion resistance of rare earth monosilicates to molten calcium–magnesium–aluminosilicate at 1300 °C, Corrosion Sci. 148 (2019) 281–292, https://doi.org/10.1016/j.corsci.2018.12.032.